Potential of products from high-temperature pyrolysis of biomass and refuse-derived fuel pellets

Wojciech Jerzak[1]*, Agata Mlonka-Mędrala[1], Ningbo Gao[2], Aneta Magdziarz[1]

[1]AGH University of Krakow, Mickiewicza 30 Av., 30-059 Krakow, Poland

[2]School of Energy and Power Engineering, Xi'an Jiaotong University, Xi'an 710049, China

*Corresponding author:

E-mail address: wjerzak@agh.edu.pl

Telephone and fax numbers: +48 12 6172636 / +48 12 6175101

Abstract

The management of energy contained in waste is an important research topic. Among many high-energy wastes, pellets are produced from refuse-derived fuels (RDF) and lignocellulosic biomass. This study investigated high-temperature pyrolysis (800 ºC) of biomass and RDF pellets. Experiments were conducted in two reactors: i) on a microscale (thermogravimetric analysis) and ii) on a laboratory scale (fixed-bed reactor) to investigate the yields of the products (char, liquid fraction, and gas) and to characterise products toward their further application. ~~Using the char from RDF reduced the carbon content, whereas using the char from biomass significantly increased carbonisation.~~ The RDF char contained less carbon than the material before pyrolysis. The carbon content of the biomass char was 90%, almost twice that of the raw material. The biomass and RDF chars were chemically and physically activated to increase their specific surface areas. The chemically activated biomass char had a sorption capacity of 156.2 mg/CO_2 at 25 ºC and 0.1 MPa. The kinetics of CO_2 sorption were also examined, and the maximum uptake was observed after 2–3 min. The higher heating value of the liquid phase, including the organic condensed phase, was 28.6 and 25.8 MJ/kg for pyrolysis of biomass and RDF pellets, respectively. The pyrolysis gas composition was analysed separately for the heating and isothermal processes. Due to the high CO, CH_4, and H_2 contents, the gas from the heating stage was characterised by a much higher heating value.

Keywords: pyrolysis; fixed-bed reactor; biomass; refuse-derived fuel; CO_2 adsorption

Graphical abstract

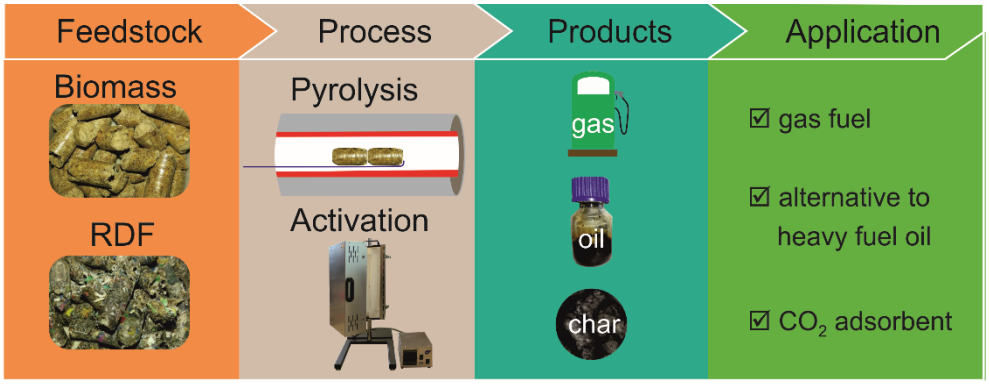

1. Introduction

The waste remaining after sorting municipal solid waste (MSW) that is unsuitable for recycling may by processed into refuse-derived fuel (RDF). ~~Storage of RDF is not recommended because of fire hazards.~~ Unfortunately, the amount of RDF produced in Poland is still greater than the possibility of using it for energy purposes in cement and waste incineration plants [1]. RDFs and biomass are calorific wastes, which in European Union (EU) legislation are partly classified as renewable sources because their combustion reduces the landfilling of waste. The need for thermal recovery of the municipal waste energy fraction has been included in the national waste prevention program [2]. The RDF was pelleted to increase the energy density and facilitate handling, transport, and storage. The same goal applies to pelleting shredded woody biomass [3]. After pelleting, biomass and RDF are characterised by low moisture and regular shape, size, and composition, which favours their future use for energy purposes.

The global production of biomass pellets is 40.4 million tons, nearly 45% of which is in the EU. Poland ranks sixth in the EU with 1.3 million tonnes per year. The RDF obtained annually from MSW is approximately 5 million tons, including 2.7 million tons thermally used (mainly cement plants), while approximately 2.3 million tons of the combustible fraction of municipal waste is disposed of in landfills [4,5]. The availability of biomass pellets and MSW for RDF production in Poland is shown in Figs. 1a and 1b, respectively.

Biomass and RDF pellets are potential raw materials for energy production or for producing valuable materials [6,7]. Thermal methods of biomass and RDF utilisation include combustion, torrefaction, gasification, and pyrolysis. However, biomass combustion can encounter operational problems, such as slagging and ash

fouling. Biomass ash contains alkali metals and chlorine, which accelerate corrosion. In turn, biomass torrefaction is a technology that works well on a laboratory scale, but requires overcoming difficulties related to increasing the scale of production. Biomass valorisation by gasification is a technology that is used to produce syngas with a high hydrogen content. The main problem that prevents the commercialisation of the gasification process is the formation of tars, their decomposition, and carbon deposition. Pyrolysis of biomass and RDF pellets is a promising thermal conversion method that has been intensively studied in recent years [8–11]. Zhou et al. [8] observed that an increase in the pyrolysis temperature of RDF pellets above 400 ºC intensifies the shrinkage phenomenon due to a decrease in the viscosity and surface tension of the plastic liquid. Char, oil and gas are produced from pyrolysis. The yields of pyrolysis products and their compositions depend, among others, on the feedstock characteristics, process temperature, and solid residence time [9,10]. There are four pyrolysis types flash, fast, intermediate and slow. The choice of flash and fast pyrolysis is aimed at obtaining a high oil yield. In the case of intermediate pyrolysis, the yields of all products are comparable. In turn, when the expected products are gas and char, slow pyrolysis will be suitable. Pyrolysis of low-moisture RDF pellets is highly recommended because it minimises the energy required for the process [11]. As the pyrolysis temperature of the biomass and RDF pellets increases, the char and oil yields decrease [9,12]. Simultaneously, the pyrolysis gas yield increases from 30% at 400 ºC to 82% at 1000 ºC [12]. The benefits of pyrolysis gas include a high heating value between 19.5–28.4 MJ/m^3, which allows its use in both the heating and the energy consumption sectors, e.g., cement and metallurgy [13]. Using high pyrolysis temperatures also implies the carbonisation of char from biomass pellets, even 93% carbon at 1000 ºC [14]. The opposite trend was observed during the pyrolysis of RDF

pellets [10,15], likely due to the higher ash content of the RDF compared to biomass. Another parameter of the pyrolysis process is the solid residence time, which has been studied to a lesser extent. Extending the solid residence time from 30 to 150 min reduces the yield of biomass char [16]. However, the solid residence time affected the char yield less as the operating temperature increased. RDF pellets contain a high percentage of plastics; therefore, the time and temperature of pyrolysis play important roles. A solid residence time of 30 min was sufficient at 500 ºC, regardless of the percentage of polyethylene in the composition of the RDF pellet, as indicated by Zaini et al. [17].

One of the key aspects of pyrolysis is the potential application of chars. Husain et al. [18] proposed using char obtained from biomass pellet pyrolysis at 600 ºC for energy production and soil remediation. The char produced by the pyrolysis of biomass pellets is microporous (average pore size less than 2 nm) and can be used as activated carbon [19]. Char obtained from wood can also be used as an additive to improve the quality of wood pellets and increase the energy density to 13.3 GJ/m^3 [20]. The positive correlation between pyrolysis temperature and the Brunauer–Emmett–Teller (BET) surface area of biomass chars was confirmed by Quan et al. [21]. However, a higher pyrolysis temperature does not always favour the largest specific surface area of the chars. The surface area of the wheat straw char at 700 ºC was lower than at 600 ºC [22]. High-temperature biomass pyrolysis (at 1400 ºC) may result in the partial melting of ash and blocking of pores in the char [23]. The residence time of the samples in the pyrolysis reactor also affected the specific surface area. An excessively long pyrolysis time of the raw material resulted in the collapse of the char pore structure, and the specific surface area was reduced [16]. The typical solid residence time of the samples in a fixed-bed pyrolysis reactor to obtain char was 30 min to 4 hours [17,24]. Therefore,

char production experiments were conducted using shorter residence times. Another popular applications of char are: i) as a porous carbon material for CO_2 capture [25], i) for supercapacitor applications [26] and i) as a potential in electrode material [27]. Modifications using thermal and chemical methods are recommended to increase the specific surface area of the chars and the CO_2 adsorption capacity. Depending on the type of biomass, the chars after physical modification were characterised by adsorption of CO_2 of 49.29 to 136.43 mgCO_2/g of char (at 25 ºC, 1 bar) [28]. Under the same conditions, the CO_2 adsorption capacity of chars treated with chemical activation ranges from 26 (modified with NH_3) to 326.55 mgCO_2/g (KOH activation at 900 ºC) [24,28].

The main goal of this study was to utilise biomass and RDF pellets via high-temperature pyrolysis. One research hypothesis proposed that chars from RDF and biomass pellets are good candidates as adsorbents for CO_2 capture. The novelty of this work is the use of a short pyrolysis time of 10 min (5 min of heating and 5 min of holding at 800 ºC) compared to the times reported in the literature which ranged from 30 min to several hours. To the best of our knowledge, using char from biomass and RDF pellet pyrolysis as a material for CO_2 adsorption has not yet been studied.

2. Materials and methods

2.1. Feedstock

This study investigated two types of pellets (biomass and RDF), which differed in their origin and the chemical composition of feedstock. Biomass pellets were produced from pine sawdust waste in an installation located on a sawmill. The pellet diameter was 6 mm, and their lengths were irregular, ranging from 7 mm to approximately 30 mm. RDF pellets (consisting of paper, plastic, textiles, wood, rubber

and cardboard) were purchased from a waste processing plant in Lesser Poland, Voivodeship.

The proximate and ultimate analyses are presented in Table 1. The high content of volatile matter (VM > 81% by weight) in both types of pellets indicates that these wastes are good candidates for thermal processes such as pyrolysis. These pellets differed significantly in terms of ash content, biomass (0.3%), and RDF content (13.3%). The ash content affects the char mass. The significant ash content in RDF may influence the reactivity of the sample through the catalytic effect of the elements present in the ash [29]. Therefore, the composition of the ash was determined using XRF, and the results are summarised in Table S1 (Supplementary Materials). The main oxides identified in the biomass ash were CaO and K_2O (approximately 66%), whereas those in the RDF ash were CaO and SiO_2 (approximately 58%). The biomass pellets contained 47.3% carbon, 6.2% hydrogen, and 0.03% sulphur. The carbon content in the RDF pellet was 10% higher than that in the biomass because of the high plastic and paper materials content [17]. The lower nitrogen content in biomass pellets is beneficial from the perspective of environmental protection because of reduced NOx emissions during thermal processes. Chlorine is an undesirable element in RDF, constituting 0.9% in pellets and 6.5% in ash, and may indicate the presence of polyvinyl chloride (PVC) [30]. Ultimate analysis of the biomass pellets indicated a higher oxygen content than the RDF pellets.

2.2. Research methodology

The research plan is illustrated in Fig. 2. For air-dried basis pellets, proximate and ultimate analyses, infrared spectroscopy with a Fourier transform, and thermogravimetric analysis of the pyrolysis process were performed at three heating rates. Preliminary investigations of the feedstocks included a thermogravimetric

analysis (TGA) performed using a Mettler Toledo STA instrument. The pyrolysis process of heating the sample to 800 ºC at rates of 5, 25, and 50 ºC/min was analysed, and the sample was held at 800 ºC for 5 min. This study aimed to determine the effect of the heating rate on the weight loss of a sample. Pyrolysis was performed using approximately 5 mg of the feedstock at a nitrogen flow rate of 50 ml/min.

The main pyrolysis process was conducted in a fixed-bed reactor at 800 ºC. The experimental setup and temperature profile of the pyrolysis process are shown in Fig. 3 and Fig. S1 (see supplementary material). The experimental pyrolysis procedure included the following steps: An approximately 5 g sample was inserted into the cooling jacket, which was purged with high-purity nitrogen for 4 min to remove air. The nitrogen flow rate was 500 ml/min, as measured using a digital mass flow meter manufactured by Aalborg. The sample was heated to a temperature of 800 ºC for no more than 5 min, and then held at this temperature for another 5 min. The final step involved sample cooling. The liquid phase (a mixture of condensed hydrocarbons and water) was collected in an ice cooler, and the non-condensed gases were transferred to a Tedlar bag for chromatographic analysis. The gas was collected separately during heating (green area in Fig. S1) and when the pellet was maintained at a constant temperature (red area in Fig. S1). The gas compositions were analysed using an Agilent 7890A gas chromatograph (GC). Additional details regarding the experimental pyrolysis process are described elsewhere [31].

Proximate and ultimate analyses, and infrared spectroscopy with a Fourier transform, were performed for the char and liquid fractions. The liquid product included a mixture of organic condensate (OC) and aqueous condensate (AC). The OC and AC were separated from the liquid fraction gravimetrically. Combustion of OC in an air

atmosphere at a flow rate of 50 ml/min was assessed using thermogravimetry for three heating rates of 5, 10, and 20 ºC/min.

The biomass and RDF chars were physically and chemically activated using steam and potassium hydroxide, respectively. The physical activation process in an atmosphere of water vapour (a mixture of H_2O heated to 300 ºC and N_2 carrier gas) at 850 ºC was performed in a fixed-bed system. Approximately 2–3 g of pretreated char was placed on glass wool in a quartz tubular reactor. The activation process lasted 25 min and consisted of a 15-minute heating stage, which began with heating the system from the ambient temperature to the set temperature, and a 10-minute gasification stage at 850 ºC. The flow rates of the process gases were 1 ml/min of water vapour and 80 ml/min of N_2.

The chars obtained during pyrolysis were chemically activated using KOH as the activating agent. The activation process was conducted in a horizontal fixed-bed reactor. The process parameters were: 800 ºC activation temperature, 1-hour activation time, nitrogen atmosphere with a flow rate of 80 ml/min, and a 1:3 char to KOH mass ratio. A mixture of char and hydroxide was ground in a knife grinder before thermal treatment to homogenise the sample. After activation, the activated carbons were subjected to repeated rinsing in distilled water to remove KOH, and then the activated carbons obtained were dried at a temperature of 105 ºC for a minimum of 6 h.

The specific surface area and average pore diameter of the chars were determined by low-temperature nitrogen adsorption/desorption using a Micromeritics ASAP 2020 Plus version 2.0. Additionally, a Hiden Isochema IGA-001 sorption analyser was used to determine the CO_2 sorption capacity in the pressure range of 0–

1.0 MPa. The activated chars were degassed at 80 ºC for approximately 12 h before analysis.

3. Results and discussion

3.1. Thermogravimetric analysis of the pyrolysis process

Preliminary investigations involved the representation of the pyrolysis process using thermogravimetric analysis (TG and DTG). The mass losses of the samples were determined using heating rates over a wide range. Crushed biomass and RDF pellets (400–600 μm fraction size) were heated at rates of 5, 25, and 50 ºC/min and then the temperature was maintained at 800 ºC for 5 min to reflect the experimental conditions in the fixed-bed reactor. Figs. 4a–4c show the results for heating rates of 5, 25, and 50 ºC/min, respectively. A positive correlation was observed between the heating rate and final mass of the char. With increasing heating rates for biomass char, it was 16.5, 16.9, and 17.6%, respectively and for RDF char, it was 21.9%, 23.7%, and 28.8%, respectively.

The heating rate also influenced the maximum mass-loss peaks. The maximum DTG peak was observed at higher temperatures as the heating rate increased. In the case of biomass pellets, there were 345, 361, and 366 ºC for the considered heating rates. Regarding the pyrolysis of biomass pellets, the maximum peaks of mass loss from RDF pellets were at higher temperatures of 456, 481 and 486 ºC, 5, 25 and 50 ºC/min, respectively. As RDF pellets consist of various materials, several peaks reflecting the decomposition of paper, cardboard, polyethylene, or polyvinyl chloride were visible in the DTG curves. The mass losses of the samples marked in Figs. 4a–4c in the isothermal region confirm the need to keep the samples at 800 ºC for 5 min, especially at a heating rate of 50 ºC/min. The mass of the RDF pellet decreased by 1.3% after 5 min. at 800 °C for the variant, at a heating rate of 50 °C/min.

3.2. Yields of pyrolysis products in a fixed-bed reactor

The yields of the biomass and RDF pellet pyrolysis products are shown in Figs. 5a and 5b. The liquid phase included two fractions, the OC and AC. The yields of the char and liquid phases were determined by weighing, whereas the yields of the gas phase were determined from differences of up to 100%. The measuring error in the mass of the liquid fraction based on the five measurement campaigns did not exceed 6% of the value. The measuring error in the mass of the char was less than 3%. The main pyrolysis products were gas from biomass and RDF (named gas_biomass and gas_RDF) which accounted for 42% and 61%, respectively. As reported by Efika et al. [9], the non-condensable gas yield was positively correlated with the heating rate, which favoured gas production. The pyrolysis temperature of 800 ºC favoured the degassing of the pellets, cracking reactions, and gas production. The gas_RDF yield at 800 ºC was consistent with the results of Tokmurzin et al [32]. The secondary pyrolysis products in terms of yield were aqueous condensed from biomass pyrolysis (AC_biomass) and char from RDF (char_RDF). The RDF pellets contained a large amount of ash (13.3%), which may explain the higher production of char_RDF than char_biomass. While the ash is ballast, Table S1 shows that the ash from RDF is rich in silica, calcium and alumina and these elements enhance the catalytic effect during pyrolysis. Similar yields of OC_biomass and OC_RDF (3.6% and 3.9% each) were obtained. Despite their low yields, OC_biomass and OC_RDF have the potential to replace heavy-oil fuels and be used as valuable chemicals. Ultimate analyses were performed to assess the energy potentials of the chars and liquid fractions.

3.3. Characteristic of pyrolysis products

3.3.1. Ultimate analyses of chars, organic condensed (OC), and aqueous organic (AC) fractions

The elemental compositions of the liquid fractions and chars, along with their ash contents, are shown in Table 2. Char_biomass contained almost twice as much carbon as the biomass pellets (from 47% to 90.5%, respectively). Another advantage of char_biomass is its low ash and oxygen content of 2.2% and 5.1%, respectively. The carbon content in char_RDF was reduced compared to that in RDF_pellets, from 56.8% to 33.7%, i.e., the opposite trend was observed compared to biomass. The high ash content of char_RDF (62%) suggests its use as a complementary material for cement production or as a catalyst carrier in the pyrolysis process. OC_biomass and OC_RDF were characterised by carbon and hydrogen contents exceeding 50% and 10%, respectively. According to Dulong's formula [33], the higher heating values of OC_biomass and OC_RDF were 28.6 MJ/kg and 25.8 MJ/kg, respectively.

The pyrolysis products with the lowest carbon contents were AC_biomass and AC_RDF. The AC fractions contained 15%–16% carbon and 9%–10% hydrogen. Recovering the organic content from AC is economically unfeasible because of the significant water dilution. Anaerobic digestion is a prospective route for processing AC_biomass and AC_RDF to produce methane. In addition, liquid-phase fermentation with added char improves biogas production while simultaneously increasing the CH_4/CO_2 ratio [34].

3.3.2. Fourier transform infrared spectroscopy (FTIR)

The presence of functional groups in the biomass pellets, RDF pellets, and pyrolysis products was analysed using Fourier transform infrared spectroscopy (FTIR). The wavenumber range of 4000–400 cm^{-1} was divided into four parts, covering stretching and deformation vibrations for single, triple, and double bonds and the fingerprint range. The spectra of the biomass and RDF pellets are shown in Fig. 6a. In the spectral ranges 3550–3200, 3000–2840, 1760–1690, 1490–1440, 1275–1200,

1200–970 and 900–675 cm^{-1}, O–H, C–H, C=O, C–H, C–O and C–H peaks were detected, respectively [35,36]. In the RDF pellet, distinct peaks were observed at 2915 and 2849 cm^{-1} assigned to the asymmetric and symmetric stretching vibrations of C–H, the characteristic bands of polyethylene [37]. Furthermore, the important peak at 1460 cm^{-1} of the infrared spectra is attributable to the polypropylene present in the RDF. Fig. 6b presents the spectra of the chars. The flattening of the char spectra confirmed the disintegration of the organic matrix, particularly in some oxygen-containing structures. The char spectra included peaks at 3634 cm^{-1} (O–H stretching in alcohols), 2317 cm^{-1} (C≡N stretching in nitriles), 2106 cm^{-1} (C≡C stretching in alkynes), 2060 cm^{-1} (N=C=N stretching in isothiocyanates), 1994 cm^{-1} (C=C=C stretching in allenes), 979 cm^{-1} (C=C bending in alkenes), and 874 cm^{-1} (C–H bending in alkenes) [38]. The intensity of the vibration of O–H, C–O, and C–H bonds in the chars disappeared compared to that in the biomass and RDF pellets. The characteristic bands of cellulose and hemicellulose, i.e., C–O (1022 cm^{-1}) and C–H (870 and 717 cm^{-1}), respectively [39], were much weaker in the char than in the pellets. This may indicate the removal of carboxyl, hydroxyl, and carbonyl groups during pyrolysis via dehydration and decarboxylation reactions. In addition, the double and triple vibrations between carbon atoms indicated the formation of aromatic compounds.

The structural properties of the functional groups in the liquid phase are shown in Fig. 6c. The wide range of O–H stretching vibrations at 3373 cm^{-1} corresponded to the functional groups in phenols, alcohols, and acidic compounds. C–H stretching vibrations (alkanes) occur at 2920 cm^{-1} and 2851 cm^{-1} only for the OC fraction. The C=O (1699 cm^{-1}) and C=C (1638 cm^{-1}) vibrations may come from alkenes, cyclic alkenes, and aromatic compounds. In the fingerprint range, C–H bending vibrations were observed (1459, 1451, and 1374 cm^{-1}). This was consistent with alkanes and

aromatics for the OC phase. The AC phase had distinct O–H vibrations at 1365 cm^{-1}, responsible for esters, acids, and phenols. The last two peaks are bending vibrations (698 and 708 cm^{-1}) that may be associated with open-chain hydrocarbons containing four or more CH_2 groups.

3.3.3. Thermogravimetric analysis of organic condensed phase combustion

The OC phase combustion process was investigated to study the potential applications of these products. Thermogravimetry analysis (TG and DTG) was examined up to 800 °C under air atmosphere. Figs. 7a and 7b demonstrate the oxidation of OC_biomass and OC_RDF at different heating rates. The OC phase includes various chemical compounds whose release into the gas phase depends on combustion temperature. Several peaks with different intensities were observed in the DTG curves. The oxidation process was divided into three stages based on the DTG curves. Low-temperature oxidation (LTO) is the first stage, which occurred up to approximately 300 ºC. During this stage, chains of heavy compounds are cleaved and oxidised at low temperatures to produce organic compounds, including aldehydes, ketones, and alcohols. OC_RDF contained more LTO because more OC_biomass (67.7%–72.6%) than OC_RDF (42.2%–53.7%) remained at 300 ºC. This indicated that LTO was the main stage in the oxidation of OC_RDF. The next stage is called medium-temperature oxidation (MTO), which occurred up to 450 ºC (OC_biomass) and 425 ºC (OC_RDF). For each heating rate, one maximum mass-loss peak was observed for OC _RDF. These occurred 327, 337, and 331 ºC for heating rates of 5, 10, and 20 ºC/min, respectively. In the MTO stage, the maximum mass losses for OC_RDF were recorded for heating rates of 10 and 20 ºC/min. High-temperature oxidation (HTO) is the final combustion stage. The driving force is the degradation of high molecular-weight compounds [40,41]. HTO was the main mass-loss region for the

OC_biomass. HTO was the main combustion region for OC_biomass (the largest mass loss), with the peak mass losses observed at 550, 590, and 634 ºC for heating rates of 5, 10, and 20 ºC/min, respectively. The burn-out of OC_biomass was at 580 ºC for 5 ºC/min and 700 ºC for 20 ºC/min. However, OC_ RDF burned at lower temperatures.

3.3.4. Gas composition

The gas chromatography results are presented in Figs. 8a and 8b. Nine gas components were identified, with six main constituents: N_2, CO, CH_4, H_2, CO_2, and C_2H_4. Pyrolysis gas formed during the primary and secondary stages of biomass and RDF pyrolysis, cracking, and related reforming reactions. The gas compositions for the heating process to 800 ºC (marked in blue) and the isothermal process (marked in red) are shown separately. Analysis of the heating stage at 800 ºC showed that CO (35.5%) was the most abundant component in gas_biomass, while N_2 (25.8%) was the most abundant in gas_RDF. CO formation is associated with the decomposition of lignocellulosic biomass components. CO is mainly produced via cracking of C–O–C and C=O groups [42]. The percentage of CO was only higher than that of CO_2 in gas_biomass and gas_RDF during heating. Simultaneously, the cracking and reforming reactions of the C=O and COOH groups were responsible for the formation of CO_2. Chen et al. [39] found that hemicellulose was responsible for CO_2 and H_2 production, whereas lignin provided the highest CH_4 content in pyrolysis gas. RDF_gas from the heating stage contained more CH_4 (19.2%), H_2 (11.2%), CO_2 (11.0%), C_2H_4 (10.4%), and other hydrocarbons than did gas_biomass. Consequently, the calculated higher heating value (HHV) of gas_RDF was 21.7 MJ/m^3, which was higher than the HHV of gas_biomass of 12.9 MJ/m^3. The combustible gaseous components accounted for > 62 vol. % of gas_biomass and more than 63% of gas_RDF. When interpreting the isothermal stage of pyrolysis, the pyrolysis gas contained 86.6% N_2 and 82.2% N_2

for gas_biomass and gas_RDF, respectively. Therefore, the HHV of gas_biomass was six times lower, and that of gas_RDF was four times lower. Gas_RDF from the isothermal process was characterised by a higher content of each hydrocarbon than that of gas_biomass. The higher hydrocarbon content was attributed to the presence of plastics in the RDF. Gases released under isothermal conditions were associated with the thermal degradation of raw materials and the cracking of higher hydrocarbons.

3.4. Char characteristic

3.4.1. Surface area analysis and adsorption/desorption of nitrogen

The specific surface areas of the chars determined by low-temperature nitrogen adsorption are listed in Table 3. The biomass chars had larger surface areas than the RDF chars. Before activation, the surface areas were 368.0 and 37.4 m^2/g for biomass and RDF, respectively. The high ash content in char_RDF negatively affected the surface area. As a result of chemical activation, larger surface areas of char_biomass and char_RDF (1375 and 515 m^2/g) were obtained than those after physical activation (701 and 231 m^2/g, respectively).

Cumulative pore volumes were assessed using nitrogen adsorption and desorption. Adsorption is the adhesion of nitrogen gas molecules to the surface of the char and open pores, whereas desorption is their removal. The increase in the surface area was accompanied by an increase in the pore volume and a decrease in the pore diameter of the tested samples. The pores in the chars were classified as mesopores according to the IUPAC classification.

3.4.2. CO_2 adsorption on chars after activation

The CO_2 adsorption and desorption performance of activated chars were studied at 25 ºC and up to 1 MPa. The adsorption isotherm describes the relationship between the adsorption capacity and pressure under isothermal conditions and was

used to characterise the adsorption properties of the analysed porous materials. Based on the analysis of the adsorption isotherm of a given material, its structure and physicochemical properties were determined. The adsorption isotherms of the activated char_biomass and char_RDF are presented in Figs. 9a and 9b.

Presented in Figs. 9a and 9b, the Type I isotherm is also called the Langmuir isotherm and has a characteristically microporous structure. The Type I isotherm is concave to the P/P_0 axis, and the amount adsorbed approaches the limit value at P/P_0 ~ 1. Type I isotherms were obtained when the adsorption was limited to a few layers of mostly adsorbed molecules and the material contained almost no mesopores. The filling of the micropores, and therefore a large amount of adsorbed agent, was observed at relatively low pressures owing to the small pore width and high heat of adsorption. The amount of adsorbed adsorbate was mainly limited by the volume of the micropores and not by the internal surface area. In all cases, the adsorption and desorption isotherms coincided, indicating the absence of hysteresis and confirming the microporous structure of the material.

The chemical adsorption yields were noticeably better for activated char_biomass. As shown in Figure 9a, for a relative pressure of 0.1 MPa, the yield of chemically activated char was 156 mg/g and for physically activated char was 104 mg/g. This may be due to the higher affinity of CO_2 molecules for KOH-activated carbons [43]. Furthermore, a higher carbon content in the biomass chars resulted in a higher carbon content in the activated carbons obtained, which may improve the CO_2 adsorption performance of the material. Activated char_biomass, which had almost three times higher carbon content than char_RDF, was two times higher in the physically activated samples and four times higher in the chemically activated samples carbon dioxide sorption capacity. The activated char_RDF samples have a higher mineral matter content, and high

concentrations of metal oxides can cause pore clogging, which directly minimises CO_2 adsorption [44].

Activated char_biomass, compared to activated char_RDF, presented higher BET surface areas, but this was not the major parameter determining the CO_2 adsorption capacity in the case of activated carbons [43,45]. Both the Brunauer-Emmett-Teller (BET) surface area and high micropore distribution determine the CO_2 sorption performance of activated carbon [43].

Compared to other experiments, e.g., chemically activated lemon peels, comparable values of CO_2 uptake were observed, as approximately 135 mg of CO_2 were adsorbed per g of the obtained activated carbon at 25 ºC and 0.1 MPa [43]. Under similar conditions, both the chemical and physical methods yielded comparable results of approximately 100 mgCO_2/g for physically activated biomass chars and 160 mgCO_2/g for chemically activated char_biomass.

This study selected RDF as the waste material for activated carbon synthesis. RDF-derived activated carbon is a better feedstock for activated carbon synthesis and displayed an adoption performance towards CO_2 four times higher than industrial-grade biomass ash-derived feedstock [46].

In the literature, the CO_2 uptakes for different adsorbents were between 100–220 mgCO_2/g at 25 ºC compared to other adsorption materials. Therefore, biomass-derived activated carbons are promising materials for CO_2 sequestration and storage. RDF-derived ACs are not as good as biomass ACs, but the thermal upgrading of waste and the production of new value-added materials is a priority and subscribes to a circular economy concept.

A decreased process temperature improves the CO_2 adsorption performance of the activated carbons obtained [43,45].

Fig. 10 presents CO_2 adsorption and desorption kinetics. During the experiment, the pressure increased rapidly and nearly reached equilibrium within a few seconds. In all cases, the mass of CO_2 adsorbed increases sharply at the beginning of the adsorption process at a given pressure and then gradually flattened over time. Maximum uptake was observed after 2–3 min. This behaviour was characteristic of activated carbons used as CO_2 adsorbents [47,48], and makes this group of materials good candidates for CO_2 capture and storage. However, further studies on material stability and durability after cyclic adsorption and desorption processes are required.

3.5. Energy efficiency and recommendations for improvement economic viability of process

The overall energy efficiency (η) of the pyrolysis process was estimated using Eq. (1) [49]. The energies of input (E_{in}) and output (E_{out}) was expersed by Eq. (2) and Eq. (3).

$$\eta = {E_{out}}/{E_{in}} \cdot 100\% \quad (1)$$

$$E_{in} = Q_{py} + HHV_{biomass} \quad (2)$$

$$E_{out} = HHV_{char} \cdot Y_{char} + HHV_{OC} \cdot Y_{OC} + HHV_{AC} \cdot Y_{AC} + HHV_{gas} \cdot Y_{gas} + Q_{loss} \quad (3)$$

where,

Q_{py} – the heat required for the pyrolysis of biomass waste. The assumed value was 1.5 MJ/kg biomass [50].

HHV – higher heating value of feedstocks and pyrolysis products (MJ/kg),

Y – mass yield of pyrolysis products, corresponding to the value in Fig. 5 divided by 100%. Furthermore, it was assumed that the gas yield from the heating stage was 27.6% (biomass) and 36.8% (RDF).

455 Q_{loss} – is the energy loss in the pyrolysis process. In these calculations, 0,58 MJ/kg of
456 biomass was used, which reflects the heat transferred by the reactor casing to the
457 surroundings air.
458 The overall energy efficiency of biomass pyrolysis was 66.7% and for RDF 48.8%. The
459 results were considered satisfactory, considering that pyrolysis gas contains nitrogen,
460 which significantly reduces its HHV. Generally, η depends on the fraction size and type
461 of biomass, reactor type, process temperature, and sample holding time. The results
462 obtained are consistent with the values in the literature for various types of pyrolysis
463 and biomass [12,49].
464 There are several key assumptions that can increase the profitability and energy
465 efficiency of the discussed pyrolysis system. The first is the location of the pyrolysis
466 system, close to the place of production and collection of biomass waste and RDF.
467 Avoiding biomass transport reduces costs and at the same time also eliminates the
468 carbon footprint. Therefore, it is reasonable to consider a mobile installation for the
469 pyrolysis and activation of biochar. The operating costs of pyrolysis reactors and their
470 activation depend significantly on the price of the electricity with which they are
471 powered. To minimize them, it is recommended to supply the reactor system with
472 electricity generated directly from photovoltaic panels. The last important aspect is the
473 water used to cool the pyrolysis gases. To reduce water consumption, the installation
474 should be equipped with a closed water circulation cooling system. This procedure will
475 contribute to protecting the natural environment and reducing costs.

476 ## 4. Conclusions

477 The pyrolysis of biomass and RDF pellets was performed in a fixed bed reactor
478 at 800 ºC. The yield and composition of the pyrolysis products (char, liquid, and gas
479 phases) were determined. For biomass and RDF pellets, the product with the highest

yield was the gas phase (42% and 61%, respectively). The gaseous phase collected during heating to 800 ºC had a higher HHV than the gaseous phase collected while maintaining the sample temperature at 800 ºC for 5 min. The HHV of the gas from RDF pyrolysis was 22 MJ/m^3 which was almost double the HHV of the gas from biomass pyrolysis. The yield of the organic condensed phase was low at 3.6% (biomass) and 3.9% (RDF). However, these phases were promising due to the HHV values 28.6 and 25.8 MJ/kg, for biomass and RDF, respectively.

The obtained chars were characterised based on their properties for further applications. Biomass char has a very high carbon content (90%), whereas RDF char contains a low amount of carbon (34%) because some compounds are released into the gas and liquid phases. However, both chars were successfully activated to enhance their surface areas and adsorption capacities. The most favourable result was obtained for chemically activated biomass char, which had a sorption capacity of 156.2 mg/CO_2 at 25 ºC and 0.1 MPa. Despite the low CO_2 sorption capacity of activated char from RDF, thermal processing of this waste should not be abandoned, as it may contribute to the reduction of the carbon footprint.

Acknowledgements

This research was funded by the National Science Centre, Poland [grant no. 2020/39/B/ST8/00883]. For Open Access, the author has applied a CC-BY public copyright licence to any author-accepted manuscript (AAM) version arising from this submission. Part of this work was supported by the Polish Ministry of Science and Higher Education within the program “PMW” 2019-2022, grant no W48/H2020/2019".

References

[1] M. Nowak, Features of Refuse Derived Fuel in Poland – Physicochemical Properties and Availability of Refuse Derived Fuel, J. Ecol. Eng. 24 (2023) 1–9. https://doi.org/10.12911/22998993/157159.

[2] T. Arjomandi, Overview of national waste prevention programmes in Europe. Europen Environmenral Agency, Denmark, 2021. https://www.eea.europa.eu/themes/waste/waste-prevention/countries/2021-waste-prevention-country-profiles/poland-waste-prevention-country-profile-2021.

[3] T.R. Sarker, V.B. Borugadda, V. Meda, A.K. Dalai, Optimization of pelletization process conditions and binder concentration for production of fuel pellets from oat hull and quality evaluation, Biomass and Bioenergy. 174 (2023) 106825. https://doi.org/10.1016/j.biombioe.2023.106825.

[4] J. Geelen, M. Karampinis, J.-M. Jossart, Bioenergy Europe Statistical Report 2022. Pellets, Brussels, 2022. www.bioenergyeurope.org.

[5] Wiesława Domańska, Environment 2021. Statistical analyses, Statistics Poland, Warsaw, 2021. https://stat.gov.pl/obszary-tematyczne/srodowisko-energia/srodowisko/ochrona-srodowiska-2021,1,22.html.

[6] M. Kwapinska, A. Horvat, D.A. Agar, J.J. Leahy, Energy recovery through co-pyrolysis of wastewater sludge and forest residues – The transition from laboratory to pilot scale, J. Anal. Appl. Pyrolysis. 158 (2021) 105283. https://doi.org/10.1016/j.jaap.2021.105283.

[7] Z. Kaczor, Z. Buliński, S. Werle, Modelling approaches to waste biomass pyrolysis: a review, Renew. Energy. 159 (2020) 427–443. https://doi.org/10.1016/j.renene.2020.05.110.

[8] C. Zhou, Q. Zhang, L. Arnold, W. Yang, W. Blasiak, A study of the pyrolysis behaviors of pelletized recovered municipal solid waste fuels, Appl. Energy. 107 (2013) 173–182. https://doi.org/10.1016/j.apenergy.2013.02.029.

[9] E.C. Efika, J.A. Onwudili, P.T. Williams, Products from the high temperature pyrolysis of RDF at slow and rapid heating rates, J. Anal. Appl. Pyrolysis. 112 (2015) 14–22. https://doi.org/10.1016/j.jaap.2015.01.004.

[10] M. Alfe', V. Gargiulo, M. Porto, R. Migliaccio, A. Le Pera, M. Sellaro, C. Pellegrino, A.A. Abe, M. Urciuolo, P. Caputo, P. Calandra, V. Loise, C.O. Rossi, G. Ruoppolo, Pyrolysis and Gasification of a Real Refuse-Derived Fuel (RDF): The Potential Use of the Products under a Circular Economy Vision, Molecules. 27 (2022) 8114. https://doi.org/10.3390/molecules27238114.

[11] Y. Yang, S. Heaven, N. Venetsaneas, C.J. Banks, A. V. Bridgwater, Slow pyrolysis of organic fraction of municipal solid waste (OFMSW): Characterisation of products and screening of the aqueous liquid product for anaerobic digestion, Appl. Energy. 213 (2018) 158–168. https://doi.org/10.1016/j.apenergy.2018.01.018.

[12] R.F. Muvhiiwa, B. Sempuga, D. Hildebrandt, J. Van Der Walt, Study of the effects of temperature on syngas composition from pyrolysis of wood pellets using a nitrogen plasma torch reactor, J. Anal. Appl. Pyrolysis. 130 (2018) 249–255. https://doi.org/10.1016/j.jaap.2018.01.014.

[13] P. Rajca, A. Poskart, M. Chrubasik, M. Sajdak, M. Zajemska, A. Skibiński, A. Korombel, Technological and economic aspect of Refuse Derived Fuel pyrolysis, Renew. Energy. 161 (2020) 482–494. https://doi.org/10.1016/j.renene.2020.07.104.

551 [14] R. Muvhiiwa, A. Kuvarega, E.M. Llana, A. Muleja, Study of biochar from
552 pyrolysis and gasification of wood pellets in a nitrogen plasma reactor for
553 design of biomass processes, J. Environ. Chem. Eng. 7 (2019) 103391.
554 https://doi.org/10.1016/j.jece.2019.103391.

555 [15] M. Zajemska, A. Magdziarz, J. Iwaszko, M. Skrzyniarz, A. Poskart, Numerical
556 and experimental analysis of pyrolysis process of RDF containing a high
557 percentage of plastic waste, Fuel. 320 (2022) 123981.
558 https://doi.org/10.1016/j.fuel.2022.123981.

559 [16] Z. Wang, K. Liu, L. Xie, H. Zhu, S. Ji, X. Shu, Effects of residence time on
560 characteristics of biochars prepared via co-pyrolysis of sewage sludge and
561 cotton stalks, J. Anal. Appl. Pyrolysis. 142 (2019) 104659.
562 https://doi.org/10.1016/j.jaap.2019.104659.

563 [17] I.N. Zaini, Y. Wen, E. Mousa, P.G. Jönsson, W. Yang, Primary fragmentation
564 behavior of refuse derived fuel pellets during rapid pyrolysis, Fuel Process.
565 Technol. 216 (2021) 106796. https://doi.org/10.1016/j.fuproc.2021.106796.

566 [18] Z. Husain, K.B. Ansari, V.S. Chatake, Y. Urunkar, A.B. Pandit, J.B. Joshi,
567 Valorisation of biomass pellets to renewable fuel and chemicals using
568 pyrolysis: characterisation of pyrolysis products and its application, Indian
569 Chem. Eng. 62 (2020) 78–91. https://doi.org/10.1080/00194506.2019.1635047.

570 [19] D.R. Nhuchhen, M.T. Afzal, T. Dreise, A.A. Salema, Characteristics of biochar
571 and bio-oil produced from wood pellets pyrolysis using a bench scale fixed bed,
572 microwave reactor, Biomass and Bioenergy. 119 (2018) 293–303.
573 https://doi.org/10.1016/j.biombioe.2018.09.035.

574 [20] R. García, M. V. Gil, A. Fanjul, A. González, J. Majada, F. Rubiera, C. Pevida,

575 Residual pyrolysis biochar as additive to enhance wood pellets quality, Renew.
576 Energy. 180 (2021) 850–859. https://doi.org/10.1016/j.renene.2021.08.113.

577 [21] C. Quan, Y. Zhou, J. Wang, C. Wu, N. Gao, Biomass-based carbon materials
578 for CO2 capture: A review, J. CO2 Util. 68 (2023) 102373.
579 https://doi.org/10.1016/j.jcou.2022.102373.

580 [22] X. Gai, H. Wang, J. Liu, L. Zhai, S. Liu, T. Ren, H. Liu, Effects of feedstock and
581 pyrolysis temperature on biochar adsorption of ammonium and nitrate, PLoS
582 One. 9 (2014) 1–19. https://doi.org/10.1371/journal.pone.0113888.

583 [23] X. Wang, M. Zhai, H. Guo, A. Panahi, P. Dong, Y.A. Levendis, High-
584 temperature pyrolysis of biomass pellets: The effect of ash melting on the
585 structure of the char residue, Fuel. 285 (2021) 119084.
586 https://doi.org/10.1016/j.fuel.2020.119084.

587 [24] P.D. Dissanayake, S. You, A.D. Igalavithana, Y. Xia, A. Bhatnagar, S. Gupta,
588 H.W. Kua, S. Kim, J.H. Kwon, D.C.W. Tsang, Y.S. Ok, Biochar-based
589 adsorbents for carbon dioxide capture: A critical review, Renew. Sustain.
590 Energy Rev. 119 (2020) 1–14. https://doi.org/10.1016/j.rser.2019.109582.

591 [25] S. Guo, Y. Li, Y. Wang, L. Wang, Y. Sun, L. Liu, Recent advances in biochar-
592 based adsorbents for CO2 capture, Carbon Capture Sci. Technol. 4 (2022)
593 100059. https://doi.org/10.1016/j.ccst.2022.100059.

594 [26] J. Wang, Y. Xu, M. Yan, B. Ren, X. Dong, J. Miao, L. Zhang, X. Zhao, Z. Liu,
595 Preparation and application of biomass-based porous carbon with S, N, Zn,
596 and Fe heteroatoms loading for use in supercapacitors, Biomass and
597 Bioenergy. 156 (2022) 106301.
598 https://doi.org/10.1016/j.biombioe.2021.106301.

[27] L. Qian, C. Chen, Y. Lv, J. Li, X. Cao, H. Ren, M.L. Hassan, Preparation and electrochemical application of porous carbon materials derived from extraction residue of Ganoderma lucidum, Biomass and Bioenergy. 166 (2022) 106593. https://doi.org/10.1016/j.biombioe.2022.106593.

[28] A.N. Shafawi, A.R. Mohamed, P. Lahijani, M. Mohammadi, Recent advances in developing engineered biochar for CO2 capture: An insight into the biochar modification approaches, J. Environ. Chem. Eng. 9 (2021) 106869. https://doi.org/10.1016/j.jece.2021.106869.

[29] Z. Sebestyén, M. Blazsó, E. Jakab, N. Miskolczi, J. Bozi, Z. Czégény, Thermo-catalytic studies on a mixture of plastic waste and biomass, J. Therm. Anal. Calorim. 147 (2022) 6259–6270. https://doi.org/10.1007/s10973-021-10962-5.

[30] G. Gałko, I. Mazur, M. Rejdak, B. Jagustyn, J. Hrabak, M. Ouadi, H. Jahangiri, M. Sajdak, Evaluation of alternative refuse-derived fuel use as a valuable resource in various valorised applications, Energy. 263 Part D (2023) 125920. https://doi.org/10.1016/j.energy.2022.125920.

[31] W. Jerzak, M. Wądrzyk, I. Kalemba-Rec, A. Bieniek, A. Magdziarz, Release of chlorine during oat straw pyrolysis doped with char and ammonium chloride, Renew. Energy. 215 (2023) 118923. https://doi.org/10.1016/j.renene.2023.118923.

[32] D. Tokmurzin, J.Y. Nam, T.R. Lee, S.J. Park, H. Nam, S.J. Yoon, T.Y. Mun, S.M. Yoon, J.H. Moon, J.G. Lee, D.H. Lee, H.W. Ra, M.W. Seo, High temperature flash pyrolysis characteristics of waste plastics (SRF) in a bubbling fluidized bed: Effect of temperature and pelletizing, Fuel. 326 (2022) 125022. https://doi.org/10.1016/j.fuel.2022.125022.

[33] F. Wanignon Ferdinand, L. Van De Steene, K. Kamenan Blaise, T. Siaka, Prediction of pyrolysis oils higher heating value with gas chromatography-mass spectrometry, Fuel. 96 (2012) 141–145. https://doi.org/10.1016/j.fuel.2012.01.007.

[34] N. Batta, T. Sarchami, C.M. Moreira, L. Rehmann, F. Berruti, Assessment of the effects of biochar on biogas production during anaerobic digestion of aqueous pyrolysis condensate: A circular economy approach, J. Environ. Chem. Eng. 11 (2023) 109982. https://doi.org/10.1016/j.jece.2023.109982.

[35] C. Quan, Y. Zhou, N. Gao, T. Yang, J. Wang, C. Wu, Direct CO2 capture from air using char from pyrolysis of digestate solid, Biomass and Bioenergy. 175 (2023) 106891. https://doi.org/10.1016/j.biombioe.2023.106891.

[36] C. Zhou, Z. Deng, Y. Zhang, X. Li, Y. Liu, J. Fu, L. Chen, Y. Yuan, Y. Jin, J. Dai, M. Yu, C. Zhang, C. Liu, W. Ao, Y. Li, Pyrolysis of typical solid wastes in a continuously operated microwave-assisted auger pyrolyser: Char characterization, analysis and energy balance, J. Clean. Prod. 373 (2022) 133818. https://doi.org/10.1016/j.jclepro.2022.133818.

[37] A. Smoliński, K. Wojtacha-Rychter, M. Król, M. Magdziarczyk, J. Polański, N. Howaniec, Co-gasification of refuse-derived fuels and bituminous coal with oxygen/steam blend to hydrogen rich gas, Energy. 254 (2022) 124210. https://doi.org/10.1016/j.energy.2022.124210.

[38] R.M. Silverstein, F.X. Webster, D.J. Kiemle, Spectrometric Identification of Organic Compound, 7th ed., John Wiley & Sons, Inc., 2005.

[39] D. Chen, K. Cen, X. Zhuang, Z. Gan, J. Zhou, Y. Zhang, H. Zhang, Insight into biomass pyrolysis mechanism based on cellulose, hemicellulose, and lignin:

Evolution of volatiles and kinetics, elucidation of reaction pathways, and characterization of gas, biochar and bio-oil, Combust. Flame. 242 (2022) 112142. https://doi.org/10.1016/j.combustflame.2022.112142.

[40] A.G.A. Jameel, A.B.S. Alquaity, K.M.O. Islam, A.A. Pasha, S. Khan, M.A. Nemitallah, U. Ahmed, Pyrolysis and Oxidation of Waste Tire Oil: Analysis of Evolved Gases, ACS Omega. 7 (2022) 21574–21582. https://doi.org/10.1021/acsomega.2c01366.

[41] F. Campuzano, J. Ordoñez, J.D. Martínez, A.F. Agudelo, S.M. Sarathy, W.L. Roberts, Thermal decomposition characteristics of the tire pyrolysis oil derived from a twin-auger reactor: Study of kinetics and evolved gases, Fuel. 338 (2023) 127248. https://doi.org/10.1016/j.fuel.2022.127248.

[42] X. He, H. Zhu, Y. Huo, W. Wang, Study on the Formation Mechanism of the Pyrolysis Products of Lignite at Different Temperatures Based on ReaxFF-MD, ACS Omega. 6 (2021) 35572–35583. https://doi.org/10.1021/acsomega.1c05275.

[43] H. Weldekidan, H. Patel, A. Mohanty, M. Misra, Carbon Capture Science & Technology Synthesis of porous and activated carbon from lemon peel waste for CO 2 adsorption, Carbon Capture Sci. Technol. 10 (2024) 100149. https://doi.org/10.1016/j.ccst.2023.100149.

[44] N. Di Fidio, D. Licursi, M. Puccini, S. Vitolo, A.M. Raspolli Galletti, Closing a biorefinery cycle of giant reed through the production of microporous and reusable activated carbon for CO2 adsorption, J. Clean. Prod. 428 (2023) 139359. https://doi.org/10.1016/j.jclepro.2023.139359.

[45] O.F. Cruz, I.C. Gómez, F. Rodríguez-Reinoso, J. Silvestre-Albero, C.R.

671 Rambo, M. Martínez-Escandell, Activated carbons with high micropore volume
672 obtained from polyurethane foams for enhanced CO2 adsorption, Chem. Eng.
673 Sci. 273 (2023) 118671. https://doi.org/10.1016/j.ces.2023.118671.

674 [46] M. Gorbounov, B. Petrovic, S. Ozmen, P. Clough, S. Masoudi Soltani,
675 Activated carbon derived from Biomass combustion bottom ash as solid
676 sorbent for CO2 adsorption, Chem. Eng. Res. Des. 194 (2023) 325–343.
677 https://doi.org/10.1016/j.cherd.2023.04.057.

678 [47] S.H. Hong, K. Chung, G. Bang, K.M. Kim, C.H. Lee, Adsorption equilibria and
679 kinetics of CO2, CH4, CO, N2, and H2 on KOH-treated activated carbon pellets
680 up to 1000 kPa, Chem. Eng. J. 431 (2022) 133396.
681 https://doi.org/10.1016/j.cej.2021.133396.

682 [48] S. Jribi, T. Miyazaki, B.B. Saha, A. Pal, M.M. Younes, S. Koyama, A. Maalej,
683 Equilibrium and kinetics of CO2 adsorption onto activated carbon, Int. J. Heat
684 Mass Transf. 108 (2017) 1941–1946.
685 https://doi.org/10.1016/j.ijheatmasstransfer.2016.12.114.

686 [49] M.M. Hasan, M.G. Rasul, M.I. Jahirul, M. Mofijur, Fuelling the future:
687 Unleashing energy and exergy efficiency from municipal green waste pyrolysis,
688 Fuel. 357 (2024) 129815. https://doi.org/10.1016/j.fuel.2023.129815.

689 [50] W. Jerzak, M. Reinmöller, A. Magdziarz, Estimation of the heat required for
690 intermediate pyrolysis of biomass, Clean Technol. Environ. Policy. 24 (2022)
691 3061–3075. https://doi.org/10.1007/s10098-022-02391-1.

692

693 **Figure captions**

708

709

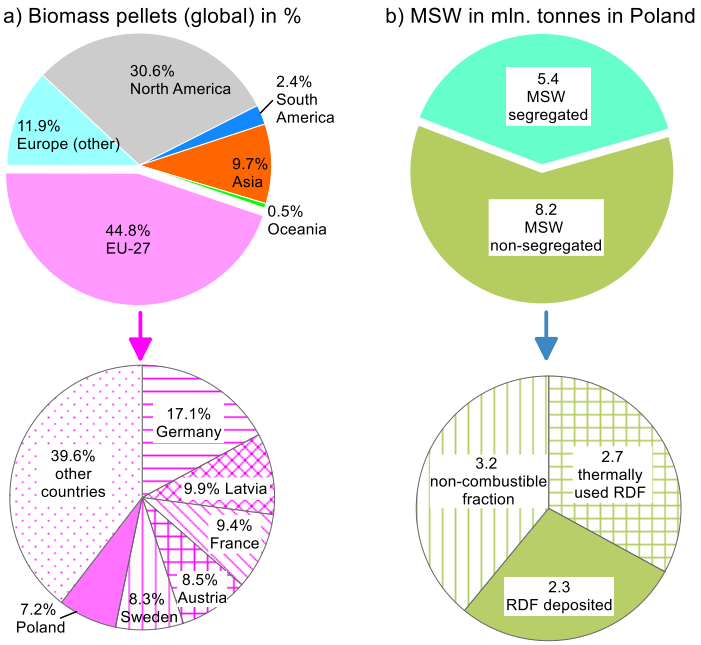

710

711 Fig. 1.

712


Types of analyzes performed:
1 Proximate analysis (A, VM, M)
2 Ultimate analysis (C, H, N, S)
3 Fourier-transform infrared spectroscopy
4 Thermogravimetric analysis
5 Gas chromatography
6 Porosimetry
7 CO2 adsorption capacity
Pyrolysis
Reactor: horizontal fixed-bed reactor
800 °C (5+5 min), N2
Physical chars activation
Reactor: vertical fixed-bed reactor
850 °C (15+10 min), H2O (at 300 °C)
Chemical chars activation
Reactor: horizontal fixed-bed reactor
800 °C (60 min), char:KOH (1:3)
Biomass
RDF
Pyrolysis
CH4
H2
Physical and
chemical
activation of chars

Fig. 2.

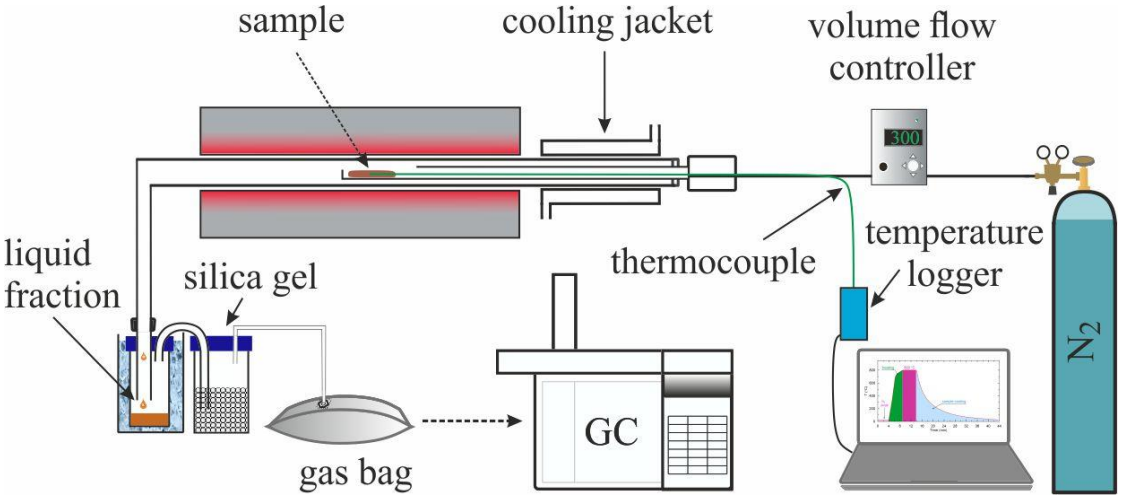
sample
cooling jacket
volume flow controller
300
liquid fraction
silica gel
thermocouple
temperature logger
N_2
GC
gas bag

715

716 Fig. 3.

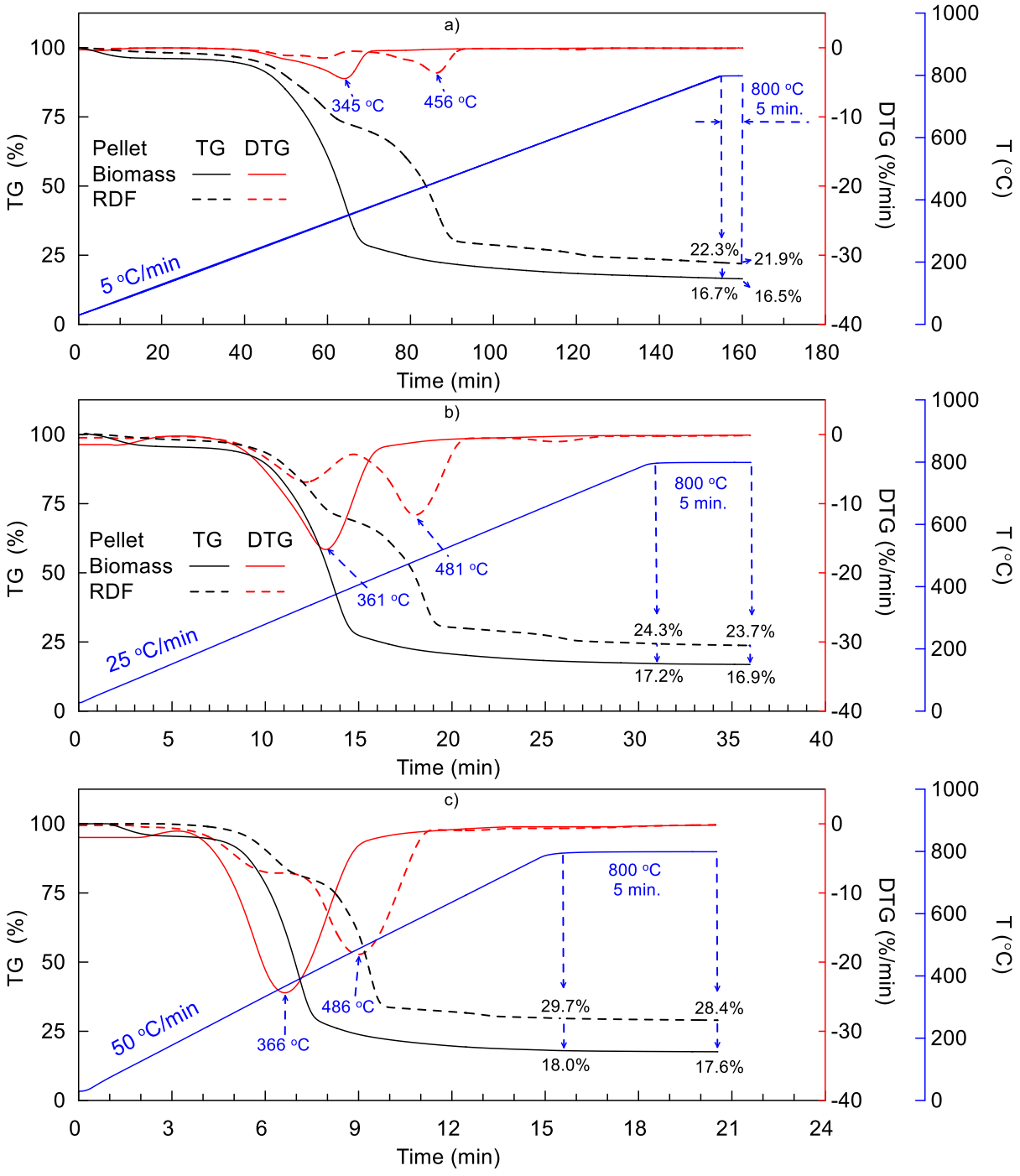
a)
TG (%)
DTG (%/min)
T (°C)
Time (min)
Pellet TG DTG
Biomass
RDF
5 °C/min
345 °C
456 °C
800 °C
5 min.
22.3%
21.9%
16.7%
16.5%
b)
25 °C/min
361 °C
481 °C
24.3%
23.7%
17.2%
16.9%
c)
50 °C/min
366 °C
486 °C
29.7%
28.4%
18.0%
17.6%

717

718 Fig. 4.

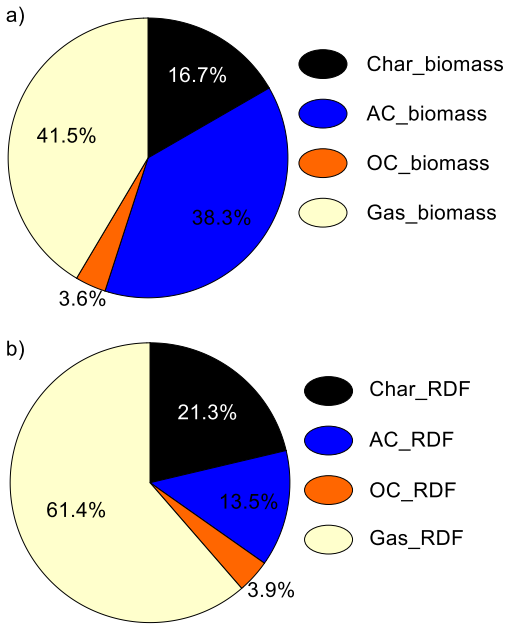
a)
16.7%
41.5%
38.3%
3.6%
Char_biomass
AC_biomass
OC_biomass
Gas_biomass
b)
21.3%
61.4%
13.5%
3.9%
Char_RDF
AC_RDF
OC_RDF
Gas_RDF

719

720 Fig. 5.

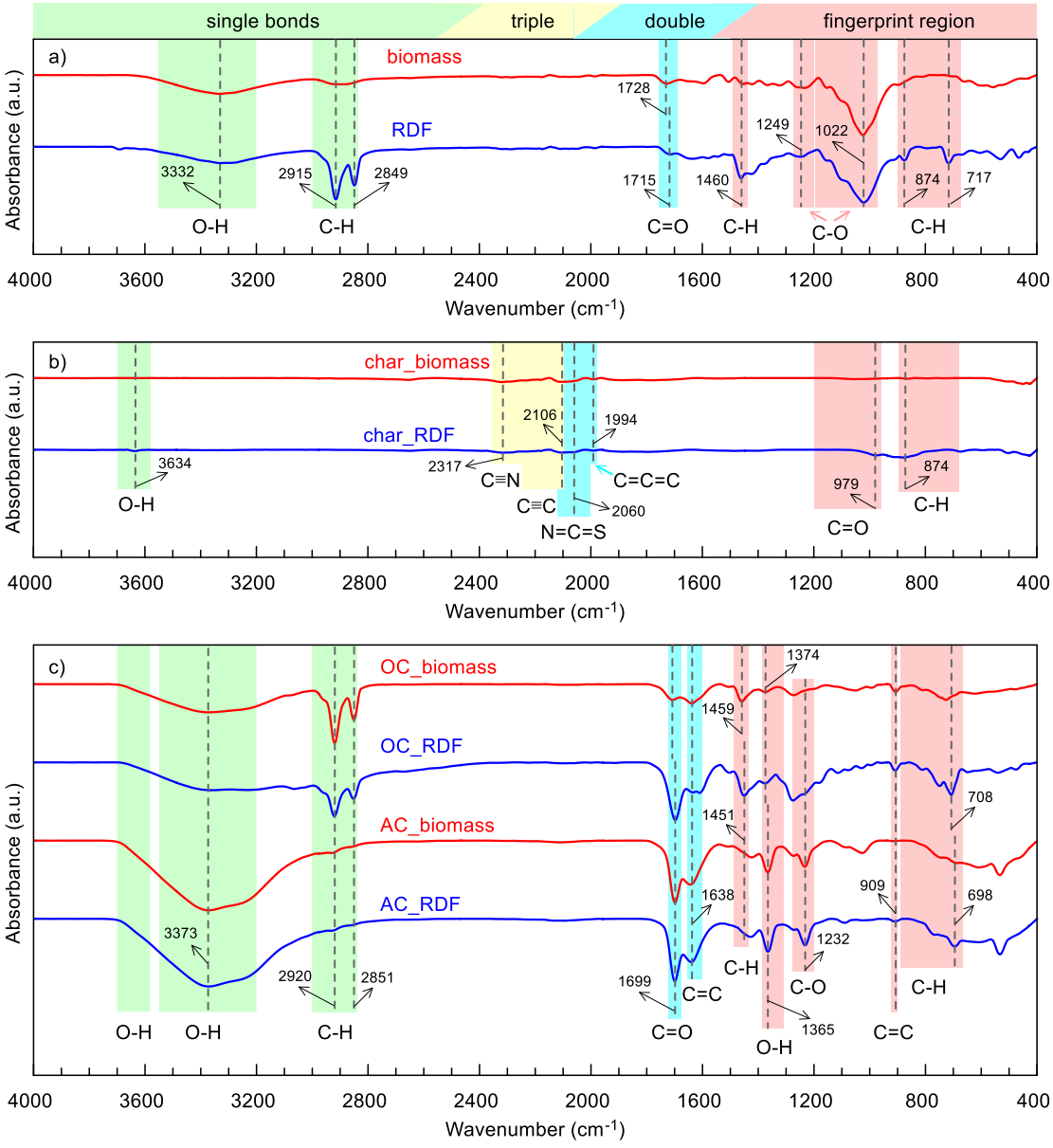
single bonds
triple
double
fingerprint region
a)
biomass
RDF
Absorbance (a.u.)
3332
2915
2849
1728
1715
1460
1249
1022
874
717
O-H
C-H
C=O
C-H
C-O
C-H
b)
char_biomass
char_RDF
3634
2317
2106
1994
2060
O-H
C≡N
C≡C
C=C=C
N=C=S
979
874
C=O
C-H
c)
OC_biomass
OC_RDF
AC_biomass
AC_RDF
3373
2920
2851
1699
1638
1459
1451
1374
1365
1232
909
708
698
O-H
O-H
C-H
C=O
C=C
C-H
O-H
C-O
C-H
C=C
4000
3600
3200
2800
2400
2000
1600
1200
800
400
Wavenumber (cm-1)

721

722 Fig. 6.

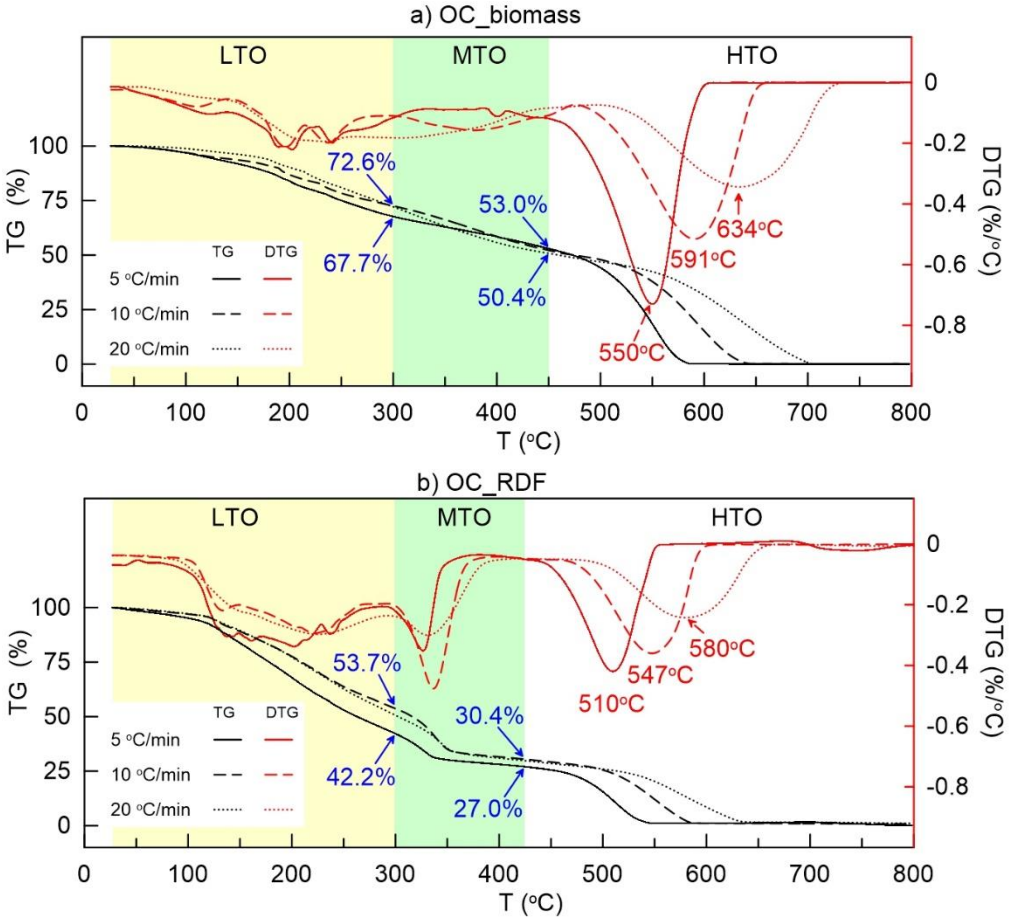
a) OC_biomass
LTO
MTO
HTO
TG (%)
DTG (%/°C)
T (°C)
TG
DTG
5 °C/min
10 °C/min
20 °C/min
72.6%
67.7%
53.0%
50.4%
634°C
591°C
550°C
b) OC_RDF
53.7%
42.2%
30.4%
27.0%
580°C
547°C
510°C

723

724 Fig. 7.

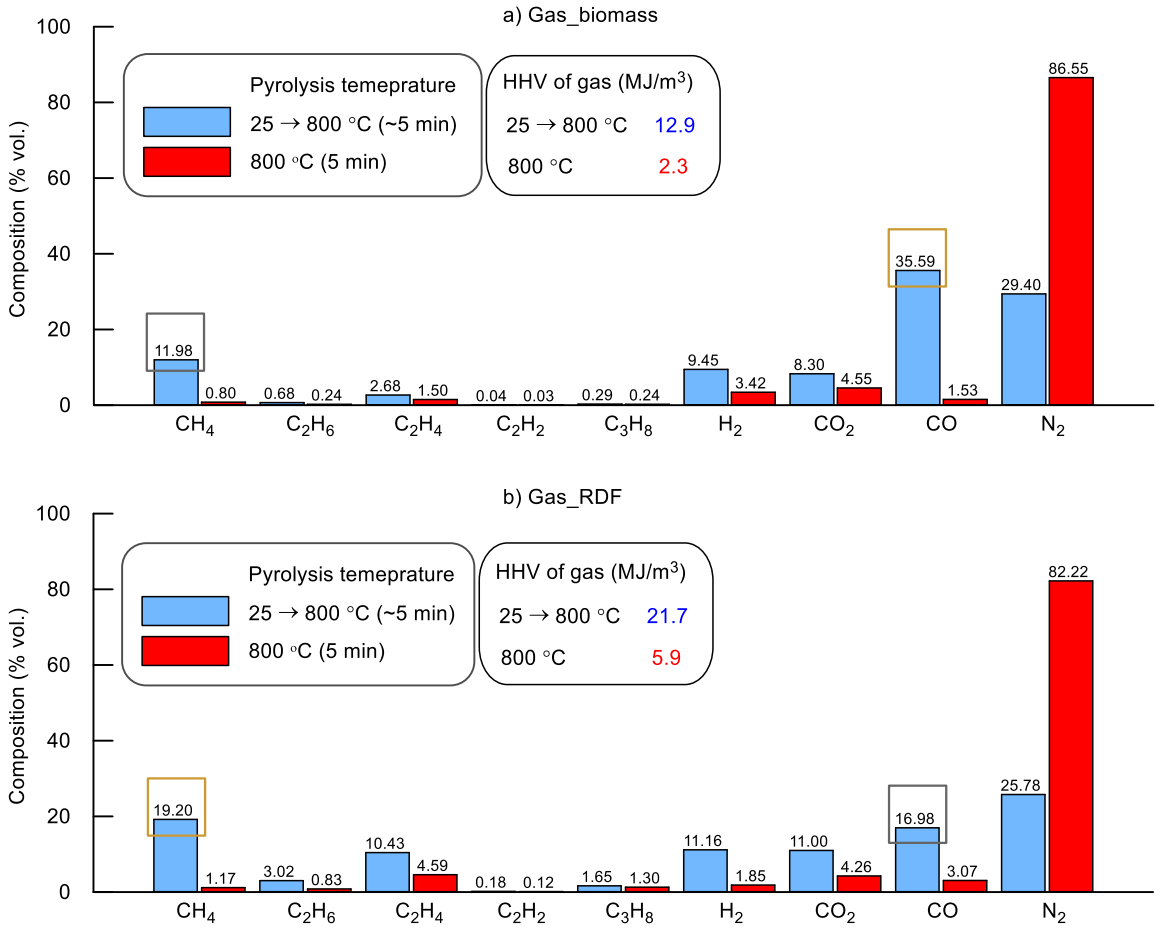
a) Gas_biomass
Pyrolysis temeprature
25 → 800 °C (~5 min)
800 °C (5 min)
HHV of gas (MJ/m3)
25 → 800 °C 12.9
800 °C 2.3
Composition (% vol.)
11.98
0.80
0.68
0.24
2.68
1.50
0.04
0.03
0.29
0.24
9.45
3.42
8.30
4.55
35.59
1.53
29.40
86.55
CH4
C2H6
C2H4
C2H2
C3H8
H2
CO2
CO
N2
b) Gas_RDF
Pyrolysis temeprature
25 → 800 °C (~5 min)
800 °C (5 min)
HHV of gas (MJ/m3)
25 → 800 °C 21.7
800 °C 5.9
Composition (% vol.)
19.20
1.17
3.02
0.83
10.43
4.59
0.18
0.12
1.65
1.30
11.16
1.85
11.00
4.26
16.98
3.07
25.78
82.22
CH4
C2H6
C2H4
C2H2
C3H8
H2
CO2
CO
N2

Fig. 8.

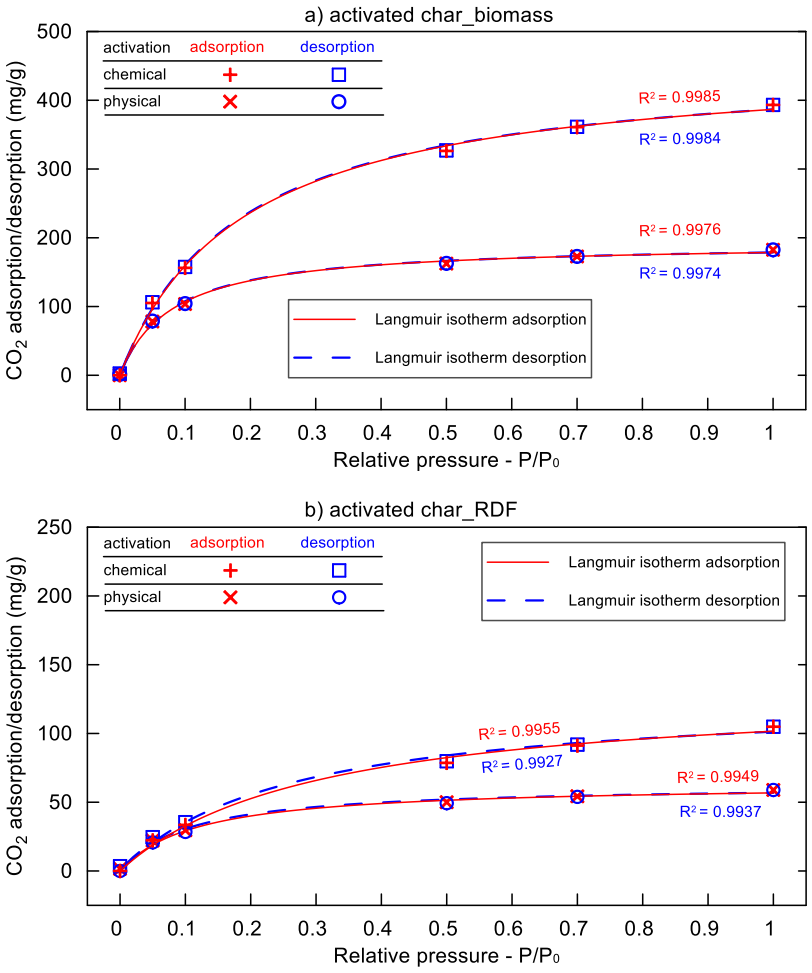
a) activated char_biomass
activation adsorption desorption
chemical
physical
R² = 0.9985
R² = 0.9984
R² = 0.9976
R² = 0.9974
Langmuir isotherm adsorption
Langmuir isotherm desorption
CO2 adsorption/desorption (mg/g)
Relative pressure - P/P0
b) activated char_RDF
activation adsorption desorption
chemical
physical
Langmuir isotherm adsorption
Langmuir isotherm desorption
R² = 0.9955
R² = 0.9927
R² = 0.9949
R² = 0.9937
CO2 adsorption/desorption (mg/g)
Relative pressure - P/P0

727

728 Fig. 9.

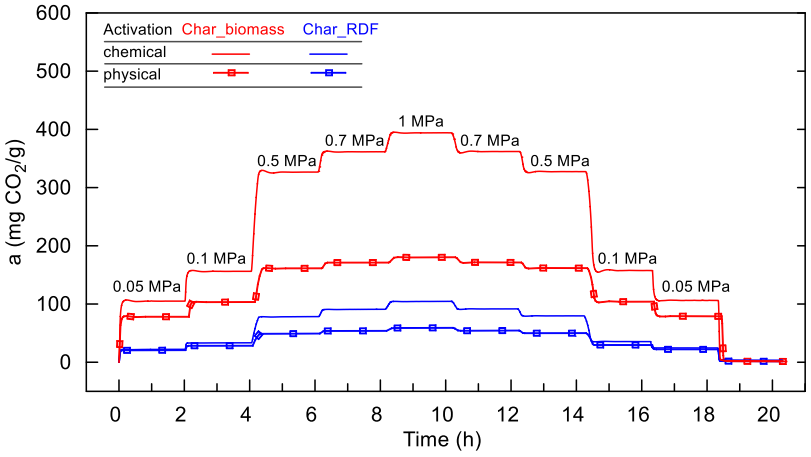

729

730 Fig. 10.